Contents lists available at ScienceDirect

Nuclear Engineering and Design

journal homepage: www.elsevier.com/locate/nucengdes

High fidelity simulations in support to assess and improve RANS for modeling turbulent heat transfer in liquid metals: The case of forced convection

Yann Bartosiewicz *

Université catholique de Louvain (UCLouvain), Institute of Mechanics, Materials, and Civil Engineering (iMMC), Louvain-la-Neuve 1348, Belgium

ARTICLE INFO

Keywords:
Liquid metal
Low Prandtl number heat transfer
High fidelity simulations (LES and DNS)

ABSTRACT

This paper attempts to give a brief overview of the work conducted through some recent EU funded projects under the Euratom research for innovative nuclear systems (THINS, SESAME and MYRTE) concerning the use of high fidelity (HiFi) simulations, namely Direct Numerical Simulations (DNS) and Large Eddy Simulations (LES), to adapt Reynolds Averaged Navier-Stokes (RANS) models for the computation of turbulent heat transfer in liquid metal flows.Here the focus is on forced convection only, that prevails in normal reactor operation, through some selected cases performed at UCLouvain, e.g. the channel flow and the impinging jet. The considered RANS approaches are those based on the simple gradient diffusion hypothesis or SGDH, and those based on the algebraic heat flux formulation (AHFM). Among the AHFM models the two possible formulations are assessed, i.e. the explicit form ($k-\epsilon-k_\theta-\epsilon_\theta$ of Manservisi and Menghini (2014) still based on the eddy diffusivity concept (gradient diffusion assumption), and the implicit form of the AHFM-NRG which is essentially a recalibration of the reference model of Kenjeres et al. (2005). The Results show the overall superiority of AHFM models, although SGDH-models using the Kay correlation for the turbulent Prandtl number and the dedicated thermal wall-function developed by Duponcheel et al. (2014) provide reasonable results at a much lower effort making them interesting for industrial applications. However further research is undoubtedly required to come closer to more universal models working for a wide range of Prandtl numbers and flow conditions.

1. Introduction

Liquid Metal Reactors (LMR) are characterized, from the thermal-hydraulic point of view, by a very low Prandtl number coolant, $Pr = \nu/\alpha \approx 0.01$, with ν the kinematic viscosity and α the heat diffusivity. At such Prandtl number, the temperature field is much smoother than the velocity field, i.e. the smallest temperature scales are much larger than those of the velocity, and, even for high Reynolds numbers, the heat transfer could be essentially molecular while the flow is fully turbulent. Consequently, simulation tools and in particular Computational Fluid Dynamics (CFD) should account for such peculiar behavior. We can classify CFD by three distinct approaches according the level of modeling/simulating the flow physics: the Direct Numerical Simulation (DNS), the Large Eddy Simulation (LES), and the Reynolds Averaged Numerical Simulation (RANS). The flow physics of interest is essentially characterized by turbulent transfers, e.g. momentum and energy transfers. Turbulent flows are characterized by a full spectrum of space and time scales, ranging from large scales, driven by the geometry and boundary conditions, down to the smallest scales where the energy is finally dissipated. This feature is illustrated by the so-called energy cascade introduced in Kolmogorov (1941) and depicted by Fig. 1 showing the turbulent kinetic energy $E(k)$ contained by eddies of size $1/k, k$ being the local wave number. Basically, the energy is injected at scales related to the geometry and boundary conditions, and this energy cascades from the large scales of the flow and dissipates at smallest scales, also called the Kolmogorov scale η, according to a law scaling as $k^{-5/3}$ (Kolmogorov, 1941) (Fig. 1). Hence the dissipation rate of the turbulent kinetic energy ϵ is set along the inertial range of the cascade, as under equilibrium conditions, the transfer rate between scales equals the dissipation rate. In this paper, the term high fidelity (HiFi) simulations refers to DNS andwell-resolved-LES. It is considered that such simulations are able to accurately capture the above mentioned peculiar behavior of heat transfer in low Prandtl fluids. Indeed, as shown in Fig. 1, DNS are supposed to resolve the full spectrum of wave numbers

* Corresponding author.
E-mail address: yann.bartosiewicz@uclouvain.be.

https://doi.org/10.1016/j.nucengdes.2021.111362
Received 14 February 2021; Received in revised form 19 May 2021; Accepted 29 June 2021

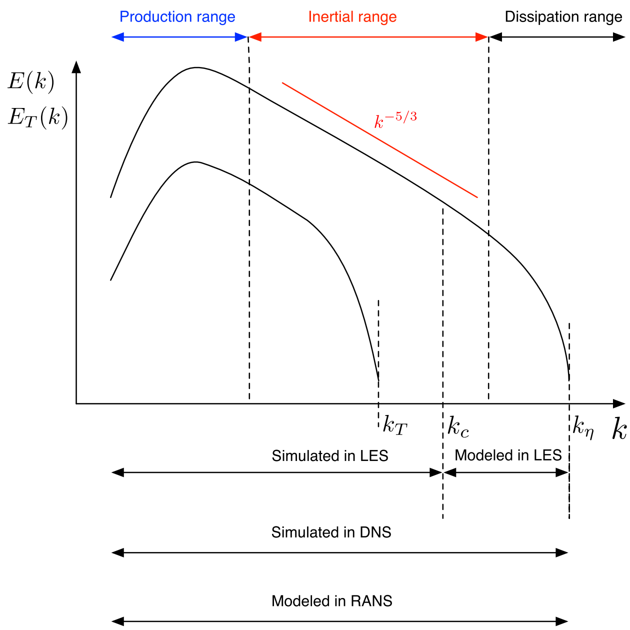

Fig. 1. Kinetic energy (E) and temperature variance(E_T) spectra for Liquid metals.

down to the Kolmogorov scale k_η, imposing a strong constraint on the mesh resolution $h_{DNS} \leqslant 2\eta$. LES explicitlyresolves the space/time scales as DNS but through a truncated space/time spectrum. This truncation ispractically imposed by the computational grid (Bartosiewicz and Duponcheel, 2019; Bartosiewicz and Duponcheel, 2017) (see next section) at a cutoff wave number $k_c = \pi/h_{LES}$. A well-resolved-LES requires $h \gtrsim 30\eta$ which is roughly the transition between the inertial range and the dissipation range. In addition, in this paper a well-resolved-LES is also a wall-resolved-LES by using an adequate subgrid model together with a wall-mesh $y+ \approx 1$.

As for the spatial scales, we can introduce the scalar diffusion cutoff length also called the Obukhov-Corrsin (Corrsin, 1951) scale η_T which is related to the Kolmogorov scale by

$$\eta_T = \left(\frac{\alpha^3}{\epsilon}\right)^{1/4} = \left(\frac{1}{Pr}\right)^{3/4} \eta_K. \tag{1}$$

Hence it is possible to relate the cutoff wavenumber for the temperature to the Kolmogorov cutoff:

$$k_T = Pr^{3/4} k_\eta, \tag{2}$$

which shows that $k_T \approx 0.03 k_\eta$ for liquid metals ($Pr \approx 0.01$). Such a temperature spectrum is overlapped on the Fig. 1 and illustrates an interesting feature. Indeed because in the offset of both spectra, there is a range of cutoff wavenumbers suitable to achieve a LES for the velocity field while resolving the smallest scales of the temperature field. In other words, it is possible to achieve a hybrid simulation which is a LES for the velocity and a DNS for the temperature (further noted in this paper as V-LES/T-DNS). In Grötzbach (2011), the author indicates the grid requirement for achieving a DNS of a temperature field, e.g. $h/\eta_T < 1$ for close to unity Prandtl number fluids, could give $h/\eta_T < 3.45$ for a liquid metal. This condition could be used *a posteriori* to check that the LES was indeed a T-DNS. In this respect, as far as well-resolved-LES are performed under the previous mentioned criterion, they can be considered as reference data (as DNS) for the turbulent heat transfer in liquid metals as a support to improve the RANS approach. Indeed as pointed out by Stieglitz and Schulenberg (2010), measuring high resolution local data in liquid metal conditions, as required for CFD grade experiments, is very challenging. Although high quality experiments become available (Shams et al., 2019d; Roelofs et al., 2015), high fidelity simulations represent a trustworthy source of diverse data for calibration and assessment of existing as well as newly RANS techniques (Roelofs, 2018; Shams et al., 2019d) in the case of liquid metal heat transfer.

Contrary to HiFi simulations, the RANS approach does not fully resolve the space/time scales of a turbulent flow, and requires models along the full space-time spectrum to mimic the turbulence. As far as turbulent heat transfer is concerned, most turbulent heat flux models rely on a structural coupling between the velocity and the temperature fields, also known as the so-called Reynolds analogy (Reynolds, 1874). As a result, the eddy diffusivity concept was naturally introduced and linked to the eddy viscosity concept by a turbulent Prandtl number (Pr_t), this approach is the so-called simple gradient diffusion hypothesis (SGDH) as explained in Bartosiewicz et al. (2013); Roelofs, 2019. It is well known that this concept, initially calibrated for fluids with $Pr \approx \mathscr{O}(1)$, fails for liquid metals (Grotzbach, 2013), as well as for some buoyant flows when the temperature variance and the ratio of the thermal to mechanical scales are important (Dehoux et al., 2012; Dehoux et al., 2012). This is the reason why the community of RANS model developers has been performing extensive researches during the last decades to not only improve the existing Reynolds analogy approach and define new best practice guidelines (BPG) (Bricteux et al., 2012; Duponcheel et al., 2014), but also to define new approaches such as implicit (Shams et al., 2014a; Shams and Santis, 2019) or explicit (4-equation model, known as $k - \epsilon - k_\theta - \epsilon_\theta$) (Manservisi and Menghini, 2014a; Manservisi and Menghini, 2014b) Algebraic Heat Flux Models (AHFM).

The objective of this paper is to give an overview of high fidelity simulations of forced convection heat transfer at low Prandtl performed at UCLouvain and how those simulations were used to (i) improve the classical Reynolds analogy for industrial calculations of wall-bounded liquid metal flows, and to (ii) qualify the above mentioned advanced AHFM-RANS models.

For more general results concerning other flow regimes such as mixed or natural convection and other test cases, the reader should refer to Roelofs (2019), Shams et al. (2019a), Shams et al. (2019d).

2. HiFi governing equations and flow solver

The governing equations are the Navier-Stokes equations for incompressible flows and the energy equation with constant physical properties, which can be written in a DNS framework as:

$$\frac{\partial u_i}{\partial x_i} = 0, \tag{3}$$

$$\frac{\partial u_i}{\partial t} + \frac{\partial u_i u_j}{\partial x_j} = \frac{\partial}{\partial x_j}\left(-P\delta_{ij} + 2\nu S_{ij}\right), \tag{4}$$

$$\frac{\partial T}{\partial t} + \frac{\partial T u_j}{\partial x_j} = \frac{\partial}{\partial x_j}\left(\alpha \frac{\partial T}{\partial x_j}\right), \tag{5}$$

where $P = p/\rho$ is the reduced pressure, ρ is the density, $S_{ij} = \frac{1}{2}\left(\frac{\partial u_i}{\partial x_j} + \frac{\partial u_j}{\partial x_i}\right)$ the strain rate tensor, T is the temperature, and α is the molecular heat diffusivity. In the numerical LES frame, these equations are projected over the LES grid, which is also called an implicitly-filtered LES or a grid-LES (see Bartosiewicz and Duponcheel, 2019). In this paper the projection operator is noted $\widetilde{(\ldots)}$ and is equivalent to a sharp Fourier cutoff. After projection of Eqs. (3)–(5) (see Bartosiewicz and Duponcheel, 2019; Bartosiewicz and Duponcheel, 2017 for details), the LES governing equations are obtained:

$$\frac{\partial \widetilde{u}_i}{\partial x_i} = 0, \tag{6}$$

$$\frac{\partial \widetilde{u}_i}{\partial t} + \frac{\partial \widetilde{\widetilde{u}_i\widetilde{u}_j}}{\partial x_j} = \frac{\partial}{\partial x_j}\left(-\widetilde{\mathscr{P}}\delta_{ij} + 2\nu \widetilde{S}_{ij} + \widetilde{\tau}_{ij}^{SGS}\right), \tag{7}$$

$$\frac{\partial \widetilde{T}}{\partial t} + \frac{\partial \widetilde{\widetilde{T}\widetilde{u}_j}}{\partial x_j} = \frac{\partial}{\partial x_j}\left(\alpha \frac{\partial \widetilde{T}}{\partial x_j} + \widetilde{\tau}_{j,T}^{SGS}\right), \tag{8}$$

with $\widetilde{\mathscr{P}} = P/\rho + \frac{2}{3}\widetilde{K}^{SGS}$, $\widetilde{\tau}_{ij}^{SGS}$ the deviatoric part of $\widetilde{\sigma}_{ij}^{SGS} = \widetilde{\widetilde{u}_i\widetilde{u}_j} - \widetilde{u_iu_j}$ and the subgrid heat flux, defined as $\widetilde{\tau}_{j,T}^{SGS} = \widetilde{\widetilde{T}\widetilde{u}_j} - \widetilde{Tu_j}$, to be modeled by the subgrid model. As mentioned in the previous section, this paper only considers well-resolved-LES which in turn can be considered as V-LES/T-DNS for low Prandtl fluids as liquid metals. In this case a subgrid heat flux model is not required or $\widetilde{\tau}_{j,T}^{SGS} = 0$.

The use of explicit filters refers to mathematical LES of explicitly-filtered LES: in this case if we apply an explicit filter $\overline{(\ldots)}$ to the instantaneous equations, the momentum equation would become for instance:

$$\frac{\partial \bar{u}_i}{\partial t} + \frac{\partial \bar{u}_i\bar{u}_j}{\partial x_j} = \frac{\partial}{\partial x_j}\left(-\overline{\mathscr{P}}\delta_{ij} + 2\nu \bar{S}_{ij} + \bar{\tau}_{ij}^{SGS}\right), \tag{9}$$

with $\bar{\tau}_{ij}^{SGS}$ is the deviatoric part of $\bar{\sigma}_{ij}^{SGS} = \bar{u}_i\bar{u}_j - \overline{u_iu_j}$. This formulation is inadequate for a grid-LES because all the terms can be solely capture on the LES grid. Indeed the product $\widetilde{u}_i\widetilde{u}_j$ contains higher frequencies than $\widetilde{u}_i$ or $\widetilde{u}_j$ alone, and would require a finer mesh to be represented. The form of Eq. 9 could be nevertheless obtained if the scale separation process used an explicit filtering only (see Sagaut, 2006), this approach could be called mathematical-LES. In this case, the residual stress appearing in the rhs of Eq. 9 would be called a subfilter stress. This subfilter stress could be then determined by partial deconvolution (see Yeo, 1987; Leonard, 1974; Carati et al., 2001). Thus the effective subgrid-scale stress in a grid-LES is not a commutator operator as it would be the case for the subfilter stress, and requires to be modeled. Moreover, if an explicit LES formulation is solved on a computational grid, it is equivalent to a double filtering operation, one explicit filter and one Fourier cutoff for the projection of the explicilty filtered equations on the grid. The result for the rhs of the momentum equation, will be a residual stress composed of a subfilter stress (deconvolvable) and a subgrid-scale stress (requiring a model). More details on explicit vs implicit filtering could be found in Bartosiewicz and Duponcheel (2017). The governing equations are discretized in space using the fourth order finite difference scheme of Vasilyev (2000), which is such that the discretized convective term conserves the discrete energy on Cartesian stretched meshes. This is an important characteristic for HiFi numerical simulations of turbulent flows to avoid additional numerical energy dissipation (Bricteux, 2008). These equations are solved using a fractional-step method. The Poisson equation for the pressure is solved using an efficient parallel multigrid solver which is either used directly or as a preconditioner for a conjugate gradient solver. The equations are integrated in time using a second order Adams-Bashforth time-stepping. At low Prandtl number, subtime-stepping is used for the temperature equation because of the very small heat conduction time-scale which is more stringent that the convective time-scale, i.e. the CFL condition. For LES, the sub-grid scale is a multiscale version of the so-called WALE model(Bricteux et al., 2009). This implementation is performed in an in-house code at UCLouvain called BigFlow. Full details about LES in liquid metals using this approach can be found in Bartosiewicz and Duponcheel (2017) and Bartosiewicz and Duponcheel, 2019.

3. How HiFi simulations improved RANS in forced convection: two selected cases

3.1. Channel flows

The periodic channel flow configuration (Fig. 2) is a generic case for

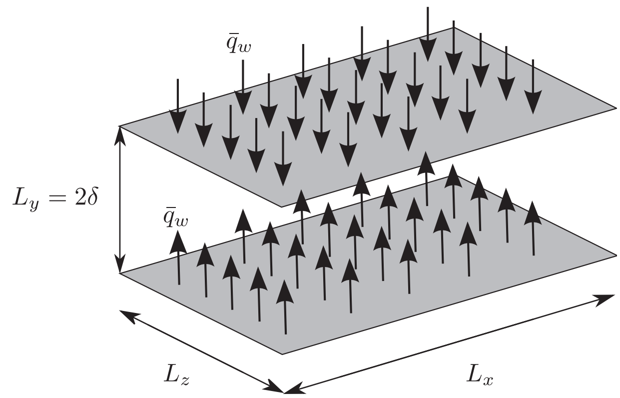

Fig. 2. Channel flow configuration. The arrows symbolize the wall heat flux.

RANS assessment of developed wall-bounded flows. This type of flow is interesting to investigate both the value of the turbulent Prandtl number in the bulk but also the near-wall heat transfer and hence the near wall modeling strategy for RANS (wall-function-RANS). At the reactor scale, this obviously applies for the flow along fuel pins as well as in any heat exchanger under normal conditions (forced convection). This case is numerically tackled by computing a time-developing flow between two plates with periodic boundary conditions in the streamwise (x) and spanwise (z) directions. The flow is characterized by the Reynolds number based on the friction velocity $\bar{u}_\tau$: $Re_\tau = \frac{\bar{u}_\tau \delta}{\nu}$ where $\bar{u}_\tau$ is related to the wall shear stress: $\bar{u}_\tau^2 = \bar{\tau}_w/\rho$, δ is half the channel width and ν is the kinematic viscosity. Furthermore, it is important to mention that the thermal boundary condition used is equivalent to imposing an averaged heat flux (not the total heat flux) or a linear temperature variation along the streamwise direction; this is achieved for a periodic flow by solving the energy equation for a modified temperature $\theta(x,y,z,t)$ (Bartosiewicz and Duponcheel, 2019):

$$T = x\frac{dT_w}{dx} - \theta, \tag{10}$$

where the wall temperature gradient forcing compensates the temperature increase in the periodic streamwise direction due to the constant mean heat flux $\{\bar{q}_w\}$ (the accolade sign stands for the mean value along the wall surface):

$$\frac{dT_w}{dx} = \frac{\{\bar{q}_w\}}{\rho c \delta \langle \bar{u}\rangle}, \tag{11}$$

where $\langle \bar{u}\rangle$ is the streamwise time and space averaged velocity (the brace sign stands for the mean value along the channel cross-section). This leads to a modified energy equation for θ with the following source term: $S_\theta = u\frac{dT_w}{dx}$:

$$\frac{\partial \theta}{\partial t} + u_j\frac{\partial \theta}{\partial x_j} = S_\theta + \alpha\frac{\partial^2\theta}{\partial x_j \partial x_j}. \tag{12}$$

The flow is driven by a streamwise pressure gradient forcing defined by $F_x = -\frac{dP_f}{dx}$, and added to the momentum equation as a source term. This pressure gradient is adapted in time so that the mass flux is kept constant.

$$\theta = 0 \text{ at } \quad y = 0 \quad \text{and} \quad y = 2\delta. \tag{13}$$

This type of boundary conditions is also named non-fluctuating thermal boundary condition, and it is more discussed in Tiselj and Cizelj (2012) and Roelofs (2019). Table 1 summarizes the different high-fidelity simulations performed at UCLouvain for this case with their corresponding reference DNS. Although a large range of Reynolds and Prandtl numbers was covered, the focus will be made here on selected results at low Prandtl number. As mentioned in the introduction, at low

Table 1
Parameters used for the channel flow simulations at UCLouvain and the reference DNS.

		Re_τ	$Re_{2\delta}$	Pr	$L_x \times L_y \times L_z$	$n_x \times n_y \times n_z$
Kawamura et al. (1999)	DNS	180	5600	0.025…1	$6.4\delta \times 2\delta \times 3.2\delta$	$128 \times 128 \times 128$
UCLouvain (Bricteux et al., 2012)	DNS	180	5600	0.01 –0.1 –1	$2\pi\delta \times 2\delta \times \pi\delta$	$128 \times 128 \times 128$
Tiselj (2011)	DNS	590	22000	0.01	$2\pi\delta \times 2\delta \times \pi\delta$	$384 \times 257 \times 384$
UCLouvain	DNS	590	22000	0.01 –0.025	$5.75\delta \times 2\delta \times 2.9\delta$	$384 \times 384 \times 384$
UCLouvain (Bricteux et al., 2012)	LES	590	22000	0.01 –0.025	$2\pi\delta \times 2\delta \times \pi\delta$	$96 \times 64 \times 96$
Kawamura (Abe et al., 2004)	DNS	640	24400	0.025	$12.8\delta \times 2\delta \times 6.4\delta$	$1024 \times 256 \times 1024$
UCLouvain (Bricteux et al., 2011)	LES	640	24400	0.01 –0.025	$2\pi\delta \times 2\delta \times \pi\delta$	$96 \times 64 \times 96$
Hoyas and Jimenez (2006)	DNS	2000	87000		$8\pi\delta \times 2\delta \times 3\pi\delta$	$6144 \times 633 \times 4608$
UCLouvain (Duponcheel et al., 2014)	*LES*	2000	87000	0.01 –0.025	$2\pi\delta \times 2\delta \times \pi\delta$	$384 \times 256 \times 384$

Prandtl numbers ($Pr \approx \mathcal{O}(0.01)$), one can take advantage of performing hybrid simulations, e.g. LES for the momentum field and DNS for the temperature field, also called V-LES/T-DNS. It worth reminding here that all LES performed were well-resolved-LES as described in the introduction and all were wall-resolved LES with a subgrid scale showing a correct asymptotic behavior. The reader is invited to check the related references for more information on the mesh resolution in each direction. Fig. 3 illustrates this V-LES/T-DNS characteristics for $Re_\tau = 590$ and $Pr = 0.01$. It is clear that the LES grid fully resolves the temperature field which depicts much larger scale structures than the velocity field. The validity of this approach is confirmed by looking at the comparison with the DNS results (Fig. 3 bottom), where both the mean temperature and its RMS are very well predicted by the LES. Another remarkable features on the mean temperature profile, are (i) the absence of any log-behavior as it is the case for the velocity profile (not shown here but in Bricteux et al. (2012)), and (ii) the unusual extension of the linear law up to $y^+ \approx 60$ which corresponds to the very lower bound of the log-profile for the velocity (Bricteux et al., 2012; Duponcheel et al., 2014). This shows the difficulty to use a direct mapping with the momentum transfer near walls by using the usual wall-function for the temperature as it is the case for RANS approach based on the full- or partial-Reynolds analogy (e.g. models based on a SGDH assumption and a Pr_t). Furthermore such simple models usually require a turbulent Prandtl number Pr_t not only for the wall-function, but also for the evaluation of the turbulent heat diffusivity in the bulk. For this point HiFi, simulations are of great value as it is possible to reconstruct the turbulent Prandtl number from high resolution results:

$$Pr_t = \frac{\nu_t}{\alpha_t} = \frac{\overline{u'v'}}{\overline{v'\theta'}} \frac{\frac{d\bar{\theta}}{dy}}{\frac{d\bar{u}}{dy}}. \tag{14}$$

Fig. 4 illustrates the results obtained by the performed HiFi simulations for Pr_t at different Reynolds numbers and for $Pr = 0.01$ (left and right) or $Pr = 0.025$ (right). It is interesting to note (Fig. 4 left) that all the curves collapse, except for $Re_\tau = 180$ which is too low to be representative of a fully turbulent flow. The turbulent Prandtl number shows a peak close to the wall and decreases to reach a plateau-like behavior in the bulk. This demonstrates the inadequacy of using a single value of $Pr_t \approx 0.85$ as in RANS based on the Reynolds analogy. However, attempting to find a relation $Pr_t = f(y^+, Pr)$ from the wall to the bulk would be also useless since very close to the wall only molecular effects yet hold (α_t should tend to zero (Duponcheel et al., 2014)) and are even dominating up to $y^+ \approx 60$ as previously observed (Fig. 3 left). As demonstrated in details in Duponcheel et al. (2014), among the tested correlation for Pr_t, that of Kays (1994),

$$Pr_t = 0.85 + \frac{0.7}{Pe_t}, \tag{15}$$

is the one which provides the best results for the tested Reynolds and Prandtl numbers. Fig. 4 (right) shows that this local correlation well envelops the Pr_t profiles obtained by the different HiFi simulations. The plateau value is generally well predicted by the correlation as well as the singular near wall behavior, which should not be an issue in codes since it will provide a turbulent heat diffusivity tending to zero.

Such HiFi simulations were also helpful to define a new temperature wall-function suited for low Prandtl numbers. By integrating the heat flux balance equation, keeping both the molecular and the turbulent component, Duponcheel et al. (2014) developed a mixed-wall-function:

$$\bar{\theta}^+ = \frac{Pr_t}{\kappa} \log\left(1 + \frac{\kappa}{Pr_t} Pr\, y^+\right), \tag{16}$$

where a value of $Pr_t = 2$ provided the best overall fit and agreed well with the observations (Fig. 4). This equation has been obtained by assuming a linear profile of the turbulent heat diffusivity $\frac{\alpha_t}{\nu} = \frac{1}{Pr_t}\kappa y^+$ away from the wall (outside the near-wal region where the turbulent heat diffusivity varies as y^{+3}) (Duponcheel et al., 2014), where $\kappa = 0.4$ and $Pr_t = 2$ provided the best fit among the different tested low-Prandtl and Reynolds numbers. This wall-function showed a better performance for low-Prandtl (Duponcheel et al., 2014) than the well-known existing blending approach of Kader (1981), which extends the linear law too far away from the wall and whose blending does not yield an accurate profile in the near-wall region, for $1 \leqslant Pry^+ \leqslant 6$, where the first grid point would be typically placed when using wall-functions. Fig. 5 (left) displays this mixed-wall-function versus the mean temperature profiles obtained by HiFi simulations at different Re_τ and $Pr = 0.01 - 0.025$. This new wall-function provides very good agreement up to $Pry^+ \approx 3$ which corresponds to $y^+ \approx 300$. The proposed new BPG for RANS based on the SGDH and Reynolds analogy is then to use the Kays correlation for Pr_t and the new mixed-wall-function. This was assessed in Duponcheel et al. (2014) and depicted in Fig. 5 (right). This plot clearly shows that using the Kays correlation significantly improves the prediction of the mean temperature profile. Furthermore, using a wall-function RANS with the mixed-wall-function and a first grid point at $y^+ = 200$ provides as good results as the same model using a wall-resolved approach with a first grid point at $y^+ \approx 1$.

As mentioned in the introduction, over the last years, more advanced RANS models were developed for simulations of liquid metals. They are essentially based either on an implicit algebraic heat flux model such as the AHFM-NRG (Shams et al., 2014a; Shams and Santis, 2019), or on an explicit variant as the $k - \epsilon - k_\theta - \epsilon_\theta$ (Manservisi and Menghini, 2014a; Manservisi and Menghini, 2014b), both being basically wall-resolved models. The main difference between these two approaches is that the AHFM-NRG model does not use the SGDH and then takes into account the non-isotropy of the heat flux, while the $k - \epsilon - k_\theta - \epsilon_\theta$ is based on the isotropic approach of the SGDH. The AHFM-NRG model has been calibrated on a wide range of operating conditions from natural convection to forced convection. In a first instance, the model constants of the original AHFM (Kenjeres et al., 2005) have been recalibrated for low-Prandtl fluids (Shams et al., 2014b) as the original model was

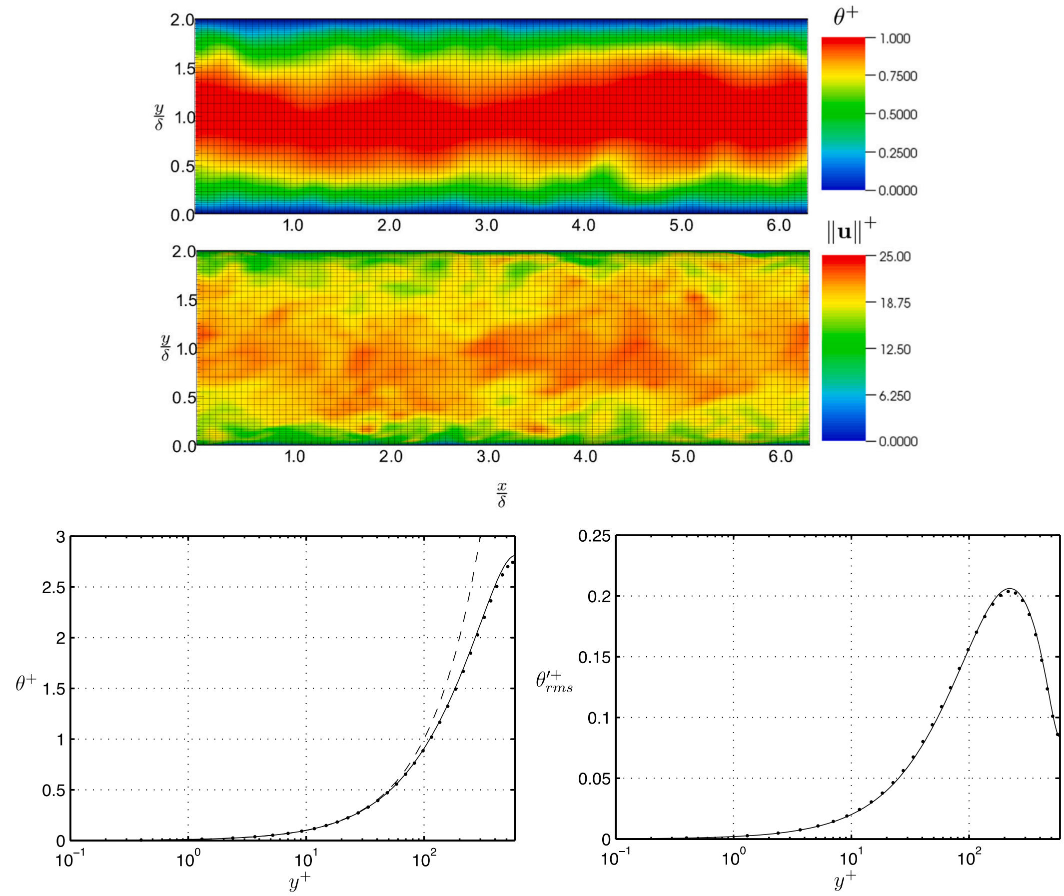

Fig. 3. $Re_\tau = 590$ and $Pr = 0.01$. Plane cut in the temperature field and in the velocity magnitude field at a given time (top). The LES grid is superimposed. Mean temperature (bottom left) and its RMS (bottom right) profiles. Present work LES (bullets), DNS (solid), theoretical near wall behaviour $\theta^+ = Pry^+$ (dash).

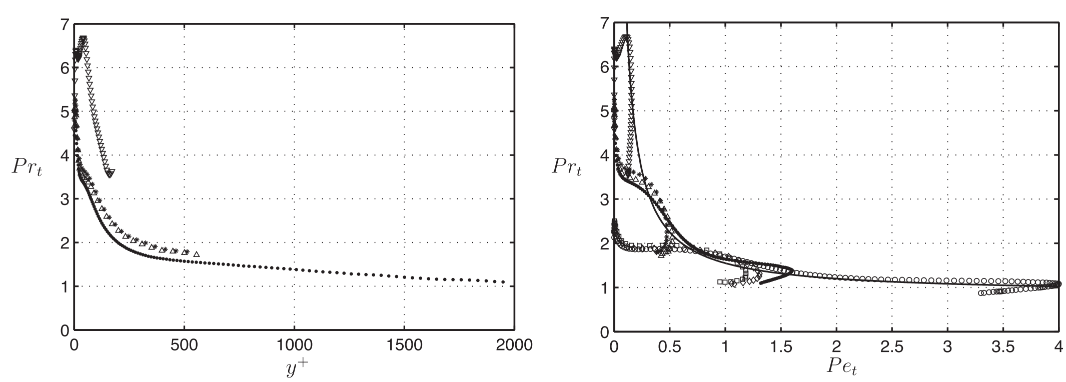

Fig. 4. Turbulent Prandtl number. Left: $Pr = 0.01$, DNS at $Re_\tau = 180$ ($\bigtriangledown$), LES at $Re_\tau = 590$ ($*$), LES at $Re_\tau = 640$ ($\bigtriangleup$), LES at $Re_\tau = 2000$ ($\cdot$). Right: Turbulent Prandtl number as a function of $Pe_t = \frac{\nu_t}{\nu} Pr$: correlation of Kays (1994) (solid line). Simulations at $Pr = 0.01$, i.e. DNS at $Re_\tau = 180$ ($\bigtriangledown$), LES at $Re_\tau = 590$ ($*$), LES at $Re_\tau = 640$ ($\bigtriangleup$) and LES at $Re_\tau = 2000$ ($\cdot$) and simulations at $Pr = 0.025$, i.e. LES at $Re_\tau = 590$ ($\square$), LES at $Re_\tau = 640$ ($\diamond$) and LES at $Re_\tau = 2000$ ($\circ$).

developed for natural and mixed convection of close to unity Prandtl number fluids; this model was names AHFM-cc (see Fig. 6). In forced convection, the value of the constant C_{t1} (related the thermal production term of the turbulent heat flux algebraic equation) has been found to play a key role and a correlation has been developed on multiple channel flow HiFi simulations (Shams et al., 2014a), $C_{t1} = 0.053 ln(RePr) - 0.27$ with $Pe = RePr > 180$. This variant model has then been named AHFM-NRG. Fig. 6 shows a selected result for the case $Re_\tau = 590$ and $Pr = 0.01$ (Bricteux et al., 2012). The AHFM-NRG clearly gives better performances for both the mean temperature as well as its RMS compared to the other versions and to a wall-resolved $k-\epsilon$ model using the partial Reynolds analogy with $Pr_t = 0.9$. It was expected since the AHFM-cc is the calibrated version of the original AHFM-2005 (Shams et al., 2014a) for forced convection and $Pr \approx 1$. Fig. 7 illustrates the same type of results for the other approach, e.g. the $k-\epsilon-k_\theta-\epsilon_\theta$ of Manservisi and Menghini (2014a). In this case the model overpredicts the LES mean temperature at $Re_\tau = 2000$ and $Pr = 0.025$ for $y^+ > 100$. This model was calibrated on the channel flow cases of Kawamura (Abe

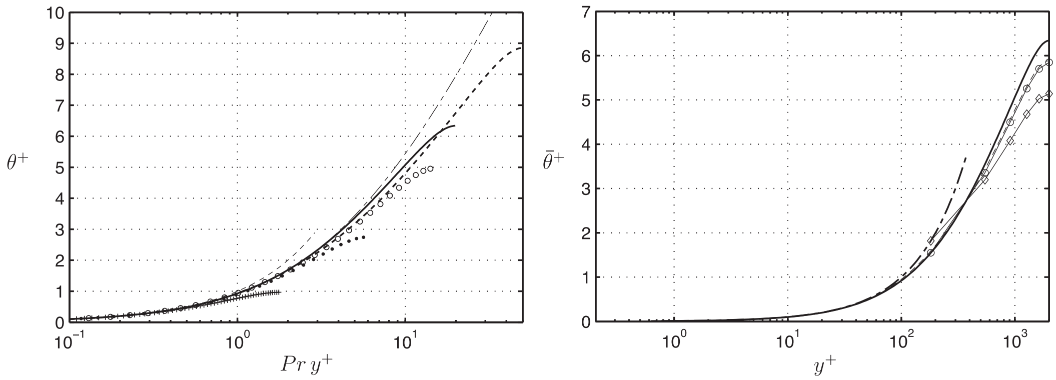

Fig. 5. Mean temperature profiles. Left: DNS at $Re_\tau = 180$ and $Pr = 0.01$ (+), LES at $Re_\tau = 590$ and $Pr = 0.01$ (·), LES at $Re_\tau = 590$ and $Pr = 0.025$ (∘), LES at $Re_\tau = 2000$ and $Pr = 0.01$ (solid) and LES at $Re_\tau = 2000$ and $Pr = 0.025$ (dash). The linear law, $\overline{\theta}^+ = Pry^+$, is plotted (thin dash) as well as the mixed law Eq. (16) (thin dash-dot). Right: $Re_\tau = 2000$ and $Pr = 0.01$, linear-law and $Pr_t = 0.85$ (thin solid and ⋄), mixed-law-wall function with $y_1^+ = 200$ and correlation of Kays (thin solid and ∘), LES (thick solid), wall-resolved RANS (OpenFoam solver as explained in Duponcheel et al. (2014)) using the correlation of Kays (thin dash), theoretical linear law, $\overline{\theta}^+ = Pry^+$ (thick dash-dot).

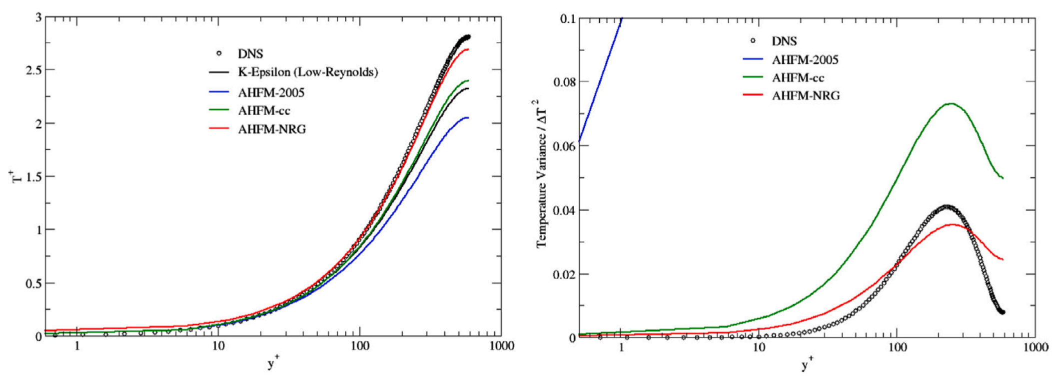

Fig. 6. Comparison of the AHFM-NRG model (implemented in STAR-CCM +) and DNS results (Bricteux et al., 2012) in the case of $Re_\tau = 590$ and $Pr = 0.01$, taken from Shams et al. (2014a).

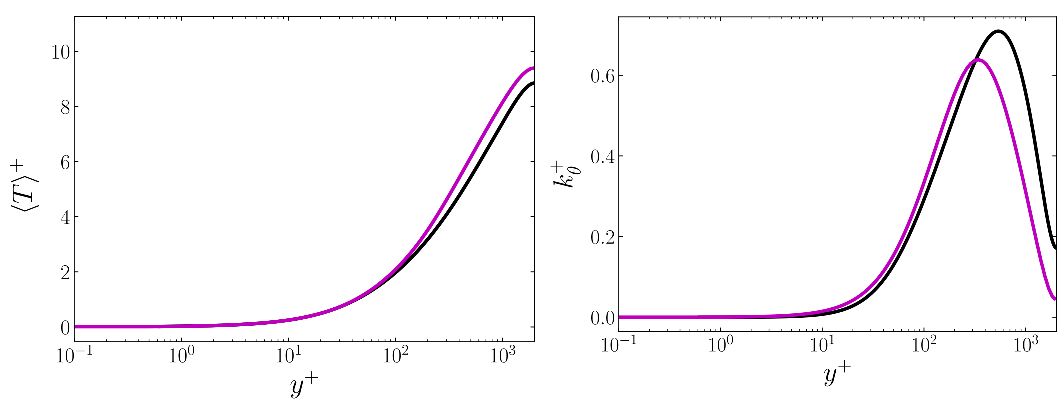

Fig. 7. $Re_\tau = 2000$ and $Pr = 0.025$. Left: mean temperature profile. Right: $k_\theta^+ = (\theta'^+_{rms})^2/2$. DNS (black), $k - \epsilon - k_\theta - \epsilon_\theta$ (magenta,implemented in OpenFoam). Taken from Ortiz (2019).

et al., 2004) up to $Re_\tau = 640$; in this case, the momentum model, more important at this Peclet number and for $y^+ > 100$ does not give more accurate results for the mean velocity profiles (see Ortiz, 2019 to see more results concerning this case). However the results are significantly improved compared to the basic approach based on the usual Reynolds analogy (Ortiz, 2019).

3.2. Impinging jet

The impinging jet (Duponcheel and Bartosiewicz, 2021) constitutes a challenging case of bounded but developing flow contrary to the channel where the flow was fully developed. The setup of the plane impinging jet consists of two infinite parallel flat plates where the top plate is split by a slit through which fluid is injected to form the jet, which impinges on the bottom plate. The problem is simulated in a rectangular box where the top ($y = H$) and bottom ($y = 0$) surfaces coincide with the walls and the top surface also contains the slit ($y = H$ and $-B/2 < x < B/2$). In the mean flow direction, far away from the jet, at $x = -L/2$ and $L/2$, convective outflow boundary conditions are used, whereas the flow is considered periodic in the spanwise direction (z), in which the domain length is W. This configuration is sketched in Fig. 8 (left). The top and bottom walls are isothermal, so that $u_i = 0$ and $T = T_w$ when $y = 0$ and when $y = H$ and $|x| \geqslant B/2$. In the slit ($y = H$ and $|x| < B/2$), the inlet jet profile is imposed. Two cases were considered: (i) a laminar inlet where a flat velocity was imposed, (ii) a turbulent inlet where a channel co-simulation was feeding a turbulent inlet velocity profile. The different cases are presented in Table 2. As the interest of this paper is to show how HiFi simulations contributed to improve/assess RANS in the case of liquid metal, and because RANS models are not suited to capture the physics of transitional flows, the selected case of interest is the T4000. In this case, the co-simulation channel is a case at $Re_\tau = 133$, which is even lower than the smallest Reynolds number ($Re_\tau = 180$) tested for the channel simulations. More details concerning the simulation parameters and results could be found in Duponcheel and Bartosiewicz (2019).

The main flow features of the T4000 case are depicted in Fig. 8

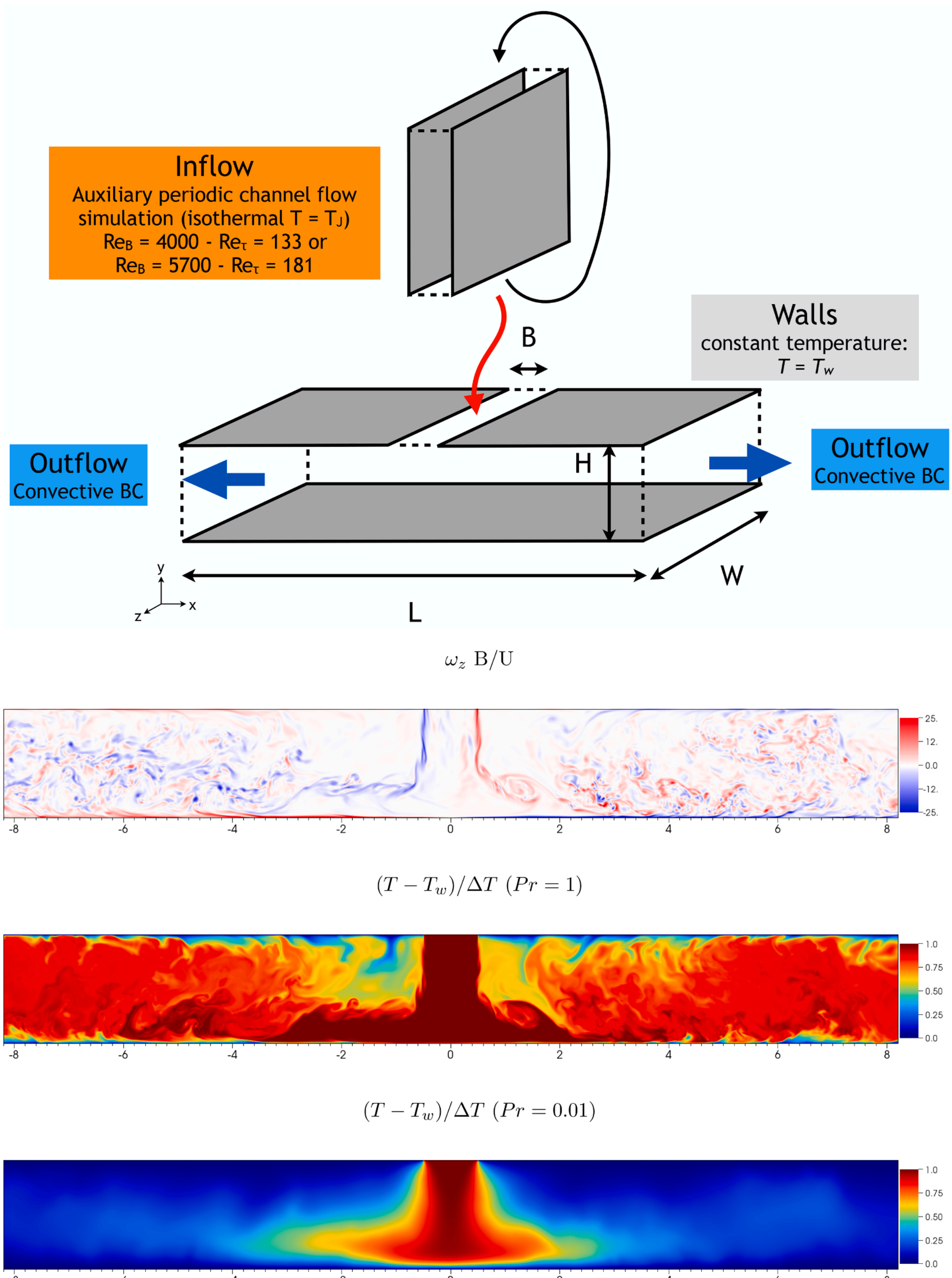

Fig. 8. Computational setup (top). Visualizations of the instantaneous flow fields in an arbitrary $x-y$ plane for the T4000 Case. Only the region $|x|/B < 8$ is shown (bottom).

Table 2
Simulation parameters for the impinging jet case.

	Re_B	Pr	$L/B \times H/B \times W/B$	$N_x \times N_y \times N_z$	Inlet
L4000	4000	1.0–0.1–0.01	$80 \times 2 \times \pi$	$2048 \times 144 \times 128$	flat laminar
T4000	4000	1.0–0.1–0.01	$80 \times 2 \times \pi$	$2048 \times 144 \times 128$	fully turbulent
T5700	5700	1.0–0.1–0.01	$80 \times 2 \times \pi$	$2560 \times 192 \times 128$	fully turbulent

(right). The velocity magnitude, the spanwise vorticity ω_z and the temperature fields at $Pr = 1$ and $Pr = 0.01$ are displayed. The turbulent fluctuations in the jet are well visible at the inlet in vorticity fields. This results in an enhanced mixing of the jet which is already well-mixed after the impingement, at around $x/B = 3$. Consequently, for the temperature at $Pr = 1$, the isothermal core at T_j does not penetrate as far as in the L4000 case (not shown), as it mixes faster. At lower Pr, the differences are less pronounced because of the smoothing effect by the higher molecular diffusivity. Here the decoupling with the momentum field as the Prandtl number is decreased is obvious. Fig. 9 shows the streamwise friction coefficient of the bottom wall, and Nusselt numbers. Elongated streamwise streaks can be seen in both the wall shear-stress and the heat fluxes across the stagnation region for $|x|/B < 3$ in the turbulent case. These streaks are not present in the L4000 case where the stagnation line is also straight and unperturbed and where the boundary layers are laminar. In the L4000 case, however, strong spanwise structures can be observed, even leading to local recirculation around $x/B = 3.75$. They are possibly related to the Kelvin-Helmholz instability of the shear layer of the jet which produces strong spanwise vortices. In the L4000 case, the transition of the boundary layers occurs around $|x|/B = 5$, where small scale perturbations of wall-friction and heat flux are seen to appear. In the turbulent T4000 case, a transition occurs between $|x|/B = 3$ and $|x|/B = 4$ where the long streaks break down into shorter structures. Regarding the heat transfer, the elongated streamwise streaks significantly increase the heat transfer locally since the maximum local heat flux in the elongated streaks in T4000 is also twice higher than the laminar heat flux obtained in L4000 (Fig. 9). As the Pr number is lowered, the Nu values are decreased and the turbulent fluctuations are smoothed. Yet, the elongated structures are still present for Pr as low as 0.01, but they are much wider than at $Pr = 1$. At $Pr = 0.01$, the Nu fluctuations in the turbulent region $|x|/B > 6$ are very small compared to the other cases where intense heat flux spots can still be observed for $|x|/B > 6$. Fig. 10 compares (for the case T4000) the different AHFM approaches based on different turbulence models for the momentum fluxes closure: the implicit AHFM-NRG based on the Lien $k-\epsilon$ (Lien et al., 1996) (Lien:NRG on Fig. 10), and the explicit AHFM of Manservisi and Menghini (2014a) based on the Launder-Sharma $k-\epsilon$ (Launder and Sharma, 1974) (LS:Manservisi on Fig. 10) as detailed in Santis et al. (2019). Moreover, the comparison is also performed with the same reference turbulence models, i.e. Lien (Lien:RA or Lien:Kays using the Kays correlation for the turbulent Prandtl on Fig. 10) and Launder-Sharma (LS:RA on Fig. 10) but using the simple gradient diffusion hypothesis (SGDH). Finally, the Elliptic Blending version of the Reynolds Stress Model (RSM-EB:RA) is also shown on Fig. 10: this model (Manceau and Hanjalic, 2002) solves a transport equation for each Reynolds stress component $\overline{u_i u_j}$, it is a wall-resolved model where the pressure strain and the dissipation rate are closed using a blending between a near-wall and a high Reynolds model. Hence this model is a combination of an anisotropic closure for the momentum fluxes and an isotropic closure for the turbulent fluxes since it uses here the Reynolds analogy. Results are presented for $Pr = 1$ (Fig. 10 left) and $Pr = 0.01$ (Fig. 10 right). At $Pr = 1$, and beyond the peak of the stagnation region, the DNS shows a plateau in the Nusselt for $3 < x/B < 5$ which turns out to become a secondary maximum at $x/B \approx 6$ for the L4000 case as illustrated in Duponcheel and Bartosiewicz (2021) and Duponcheel and Bartosiewicz (2019). For this T4000 case, the plateau corresponds to the zone where the streaks break as observed in Fig. 9, while for the laminar case the secondary maximum corresponds at the laminar-turbulent transition of the wall boundary layer (Duponcheel and Bartosiewicz, 2019). None of the tested RANS models is yet able to capture this plateau and their behavior looks closer to laminar than turbulent outside of the stagnation region. However, the $k-\epsilon-k_\theta-\epsilon_\theta$ of Manservisi and Menghini (2014a) better captures the peak in the stagnation region as well $x/B > 9$. This region is where the boundary layer has fully transitioned and where the laminar and the turbulent profiles collapse (see Duponcheel and Bartosiewicz, 2021; Duponcheel and Bartosiewicz, 2019). At $Pr = 0.01$, the Nusselt has decreased and shows a more monotonic behavior. The explicit AFM (Manservisi and Menghini, 2014a) gives again the best performance even though both the AFM-NRG (Lien:NRG) and the classical SGDH model with the Kays correlation are very close, the models based on the Reynolds analogy showing more discrepancies (RSM-EB being the best of them). Fig. 11 and Fig. 12 show the

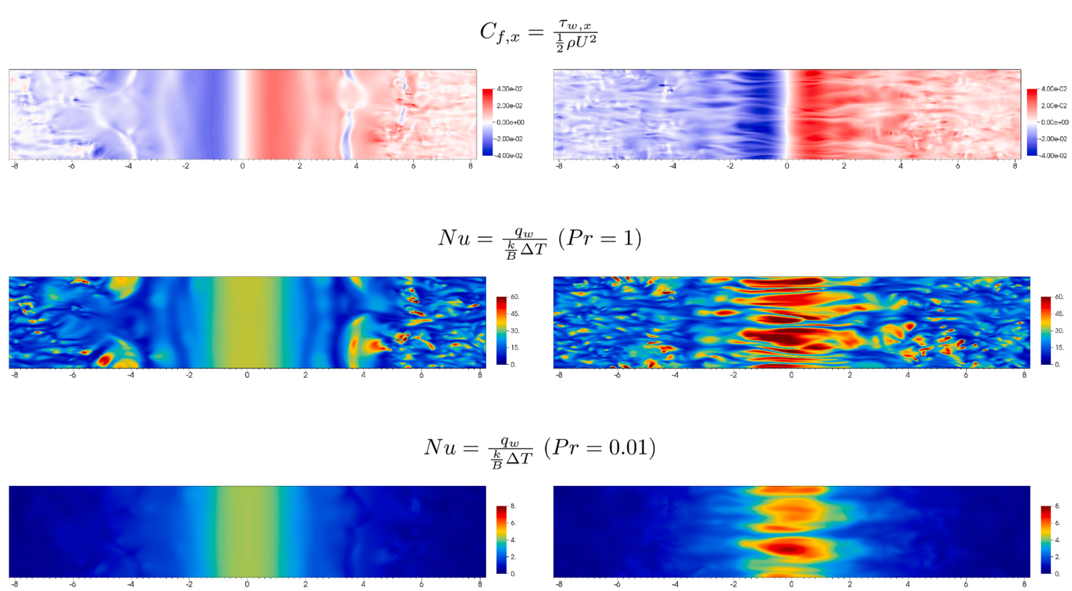

Fig. 9. visualizations of the fluxes on the bottom wall. L4000 case (left), T4000 case (right), $Pr = 1$ (top), $Pr = 0.01$ (bottom).

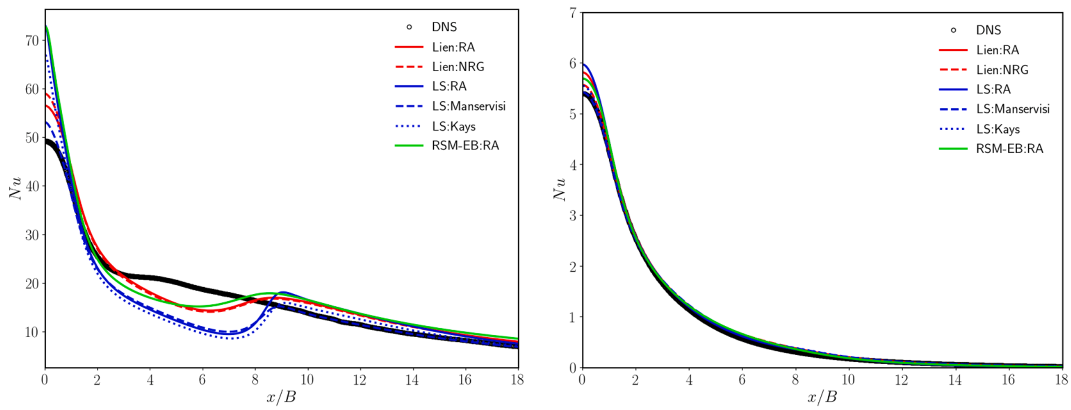

Fig. 10. Nusselt Number for the T4000 case (from Santis et al. (2019)). Left: *Pr* $= 1$. Right: *Pr* $= 0.01$. Lien-based models as well as RSM are implemented in STAR-CCM +, while LS-based models are implemented in OpenFoam.

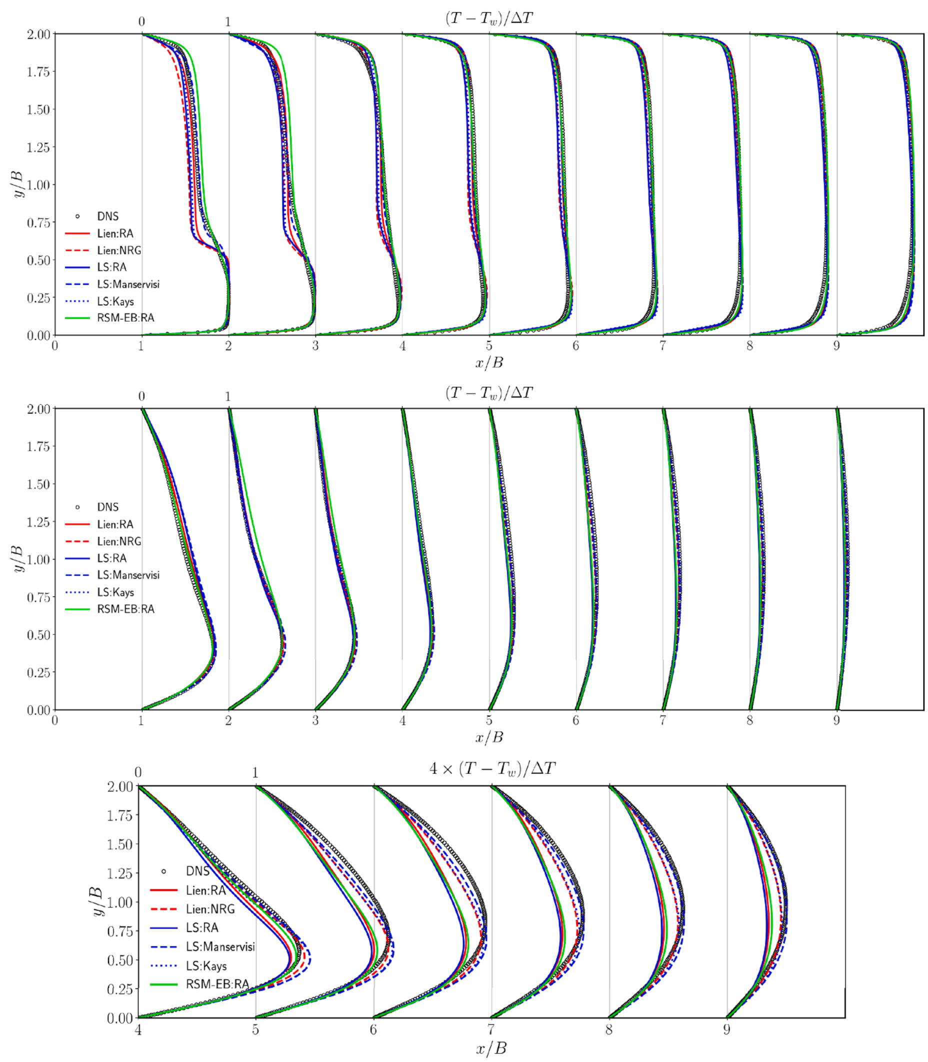

Fig. 11. T4000 case. Vertical temperature profiles (from Santis et al. (2019)). Top: *Pr* $= 1$. Middle: *Pr* $= 0.01$. Bottom: *Pr* $= 0.01$, temperature values multiplied by four to magnify differences. Lien-based models as well as RSM are implemented in STAR-CCM +, while LS-based models are implemented in OpenFoam.

comparison of the different models for the temperature profile and the turbulent heat flux at the bottom wall respectively, for *Pr* $= 1$ and *Pr* $= 0.01$. At *Pr* $= 1$ the results are essentially driven by the turbulent momentum field as the Reynolds analogy is valid, hence the turbulence model used for momentum closure is mostly important here. For such cases, the RSM-EB model gives the best overall performance, even though the profile of the vertical turbulent heat flux is not well predicted by any of the model before transition (streaks break) occurs, e.g. $x/B < 5$. At Low Prandtl, models based on the Reynolds analogy are no more suited, and dedicated developed approaches offer the best results.

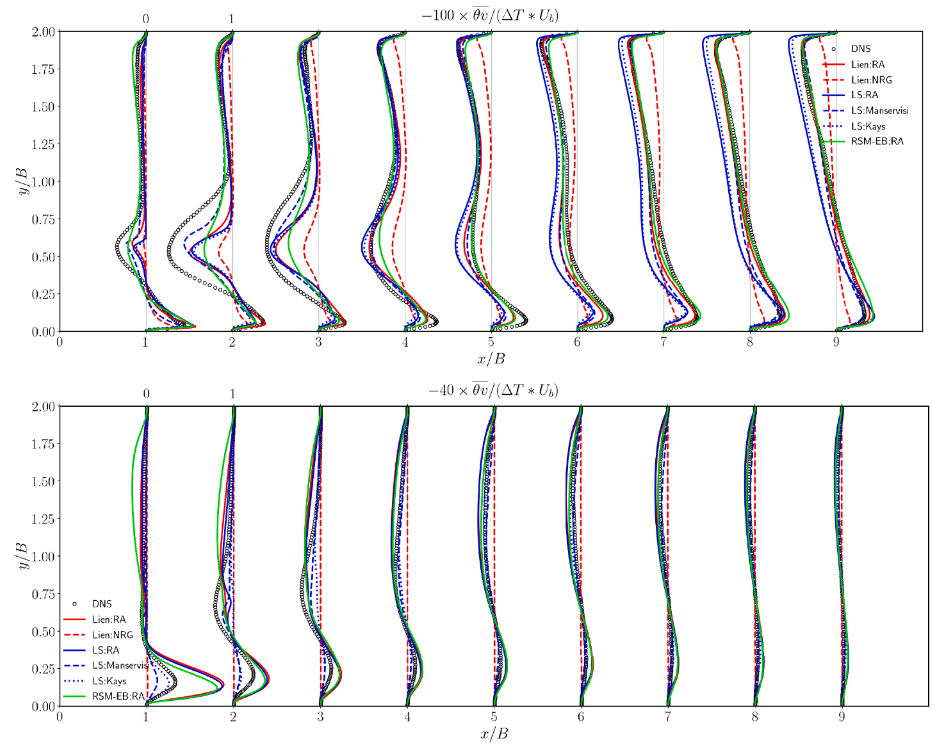

Fig. 12. T4000 case. Vertical turbulent heat flux (from Santis et al. (2019)). Top: $Pr = 1$. Bottom: $Pr = 0.01$ zoom. Lien-based models as well as RSM are implemented in STAR-CCM +, while LS-based models are implemented in OpenFoam.

Especially the $k - \epsilon - k_\theta - \epsilon_\theta$ (LS:Manservisi) is overall closer to DNS results followed by the AFM-NRG and the classical Launder-Sharma $k - \epsilon$ using the Kays correlation for the turbulent Prandtl number as advised in the previous section.

4. Conclusion

This paper provided a brief overview on the relation between HiFi simulations and the assessment and development of dedicated approaches or best practice guidelines for RANS to compute turbulent forced convection in liquid metals. This work has been achieved through three EU funded projects, e.g. THINS, SESAME and MYRTE. For a sake of brevity, the paper only focused on some selected cases which were computed at UCLouvain. However, high fidelity simulations as well as RANS tests were performed on other cases as well as in other conditions such as mixed and natural convection (Shams et al., 2019a; Shams et al., 2019d; Shams et al., 2019b). Nevertheless, the presented cases illustrated how HiFi simulations contributed to develop (i) new BPG guidelines if models based on the simple gradient diffusion hypothesis are used, and (ii) to develop and assess new approaches calibrated for low Prandtl number fluids such as the algebraic heat flux models (AHFM). In the former case (i), a simple $k - \epsilon$ based model together with the Kays correlation for the turbulent Prandtl number and the mixed-wall-function is a good candidate for industrial simulations where fine wall-meshes are not affordable because limitations of computational resources and time constraint. In the latter case (ii), AFM models (either implicit of explicit) could be a good choice in more complex situations such as mixed or natural convection or when strong turbulence anisotropy is expected (implicit AHFM-NRG). Those models bring the interested feature of being not related to the concept of turbulent Prandtl number. For explicit AHFM, although they still rely on a gradient hypothesis and then an eddy diffusivity concept, the turbulent heat diffusivity is here evaluated by solving two-transport equations for k_θ and $\epsilon_t heta$, which means that turbulent thermal diffusivity is directly correlated to the thermal characteristic time of turbulence which is itself not directly correlated to the mechanical characteristic time. However, solving an equation for ϵ_θ requires additional modeling assumptions and many other model coefficients that need to be tuned. In comparison, the implicit approach of the AHFM-NRG, allows to tackle cases when turbulent the heat flux is not aligned with the temperature gradient as it could be the case in natural convection. However this model assumes a constant thermal to mechanical time scale ratio, which is known to be questionable (Otic et al., 2005) especially and contradictory (in respect to the first targeted application of the model) in natural convection. to the author's knowledge, there is no extensive study investigating the relative importance of the assumption of the gradient hypothesis (eddy viscosity) and that of the constant time scale ratio according the flow situation, neither an attempt to combine both approaches, e.g. solving the ϵ_θ equation of Manservisi and Menghini (2014a) to be used in the AHFM-NRG to investigate the sensitivity of this time scale ratio. Moreover, the two approaches will also always depend on the turbulence model used for turbulent momentum fluxes. In this regards, in order to tackle flows where the anisotropy of turbulence could induce strong effects on momentum diffusion, which in turn would affect turbulent thermal diffusion, the use of anisotropic turbulence models such as Reynolds Stress Model (RSM) has been recently proposed as the AHFM-NRG-RSM-EB (Shams et al., 2019b). The assessment of this model is however still limited to force convection cases. Among possible issues of these models are their lack of generality and their complexity in calibration of the increasing number of model constants. Although some calibration attempts proposed to change some constants into functions (as the c_{t1} or c_{t3} constants for the AHFM-NRG and AHFM-NRG +, see Shams et al., 2019c), those functions are still dependent of global parameters such as the Reynolds, Peclet, or Rayleigh numbers, which is questionable as far as local production/dissipation terms are concerned. An interesting and emerging path to use the huge amount of local data issued from HiFi simulations, is the use of machine learning techniques to derive a general model of the turbulent heat flux components as it already exists for Reynolds stresses (Jiang et al., 2020; Sotgiu et al., 2019). In this regard, Fiore et al. (2021a); Fiore et al., 2021b paved the way to such a new approach which efficiently use the data of existing HiFi simulations while taking care to respect both mathematical and physical constraint that such turbulent heat flux models should satisfy (realizability, invariance properties, second law of thermodynamics), which is a key point when relying on data-driven methods.

CRediT authorship contribution statement

Yann Bartosiewicz: Conceptualization, Writing - original draft, Writing - review & editing, Supervision, Project administration, Funding acquisition.

Declaration of Competing Interest

The authors declare that they have no known competing financial interests or personal relationships that could have appeared to influence the work reported in this paper.

Acknowledgments

The work described in this paper has been funded by the Euratom research and training programmes under grant agreements No. 249337 (THINS, FP7), No. 654935 (SESAME, H2020),and No.662186 (MYRTE). The present research benefited from computational resources made available on the Tier-1 supercomputer of the Fédération Wallonie-Bruxelles, infrastructure funded by the Walloon Region under the grant agreement No. 1117545. Computational resources have also been provided by the Consortium des Equipements de Calcul Intensif (CECI), funded by the Fonds de la Recherche Scientifique de Belgique (F.R.S.-FNRS) under Grant No. 2.5020.11 and by the Walloon Region.

References

Abe, H., Kawamura, H., Matsuo, Y., 2004. Surface heat-flux fluctuations in a turbulent channel flow up to $Re_\tau = 1020$ with $Pr = 0.025$ and 0.71. Int. J. Heat Fluid Flow 25 (3), 404–419.
Bartosiewicz, Y., Duponcheel, M., 2017. Large eddy simulation: application to liquid metal fluid flow and heat transfer. In: Thermohydraulics and Chemistry of Liquid Metal Cooled Reactors, VKI Lecture Series, Von Karman Institute for Fluid Dynamics.
Bartosiewicz, Y., Duponcheel, M., 2019. Large eddy simulation: application to liquid metal fluid flow and heat transfer. In: Thermal Hydraulics Aspects of Liquid Metal Cooled Nuclear Reactors. Elsevier, Woodhead Publishing. pp. 245–273.
Bartosiewicz, Y., Duponcheel, M., Manconi, M., Winckelmans, G., Bricteux, L., 2013. Turbulence modeling at low prandtl number. In: Fluid Mechanics and Safety Issues in HLM Nuclear Reactors, VKI Lecture Series, Von Karman Institute for Fluid Dynamics.
Bricteux, L., 2008. Simulation of turbulent aircraft wake vortex flows and their impact on the signals returned by a coherent doppler lidar system (Ph.D. thesis). Université catholique de Louvain.
Bricteux, L., Duponcheel, M., Winckelmans, G., 2009. A multiscale subgrid model for both free vortex flows and wall-bounded flows. Phys. Fluids 21 (10), 105102 .
Bricteux, L., Duponcheel, M., Winckelmans, G., Bartosiewicz, Y., 2011. DNS and LES of turbulent channel flows at very low Prandtl number: Application to convection in lead-bismuth. In: The 14th International Topical Meeting on Nuclear Reactor Thermalhydraulics NURETH-14.
Bricteux, L., Duponcheel, M., Winckelmans, G., Tiselj, I., Bartosiewicz, Y., 2012. Direct and large eddy simulation of turbulent heat transfer at very low Prandtl number: application to lead–bismuth flows. Nucl. Eng. Des. 246, 91–97.
Carati, D., Winckelmans, G.S., Jeanmart, H., 2001. On the modeling of the subgrid-scale and filtered-scale stress tensors in large-eddy simulation. J. Fluid Mech. 441, 119–138.
Corrsin, S., 1951. On the spectrum of isotropic temperature fluctuations in an isotropic turbulence. J. Appl. Phys. 22, 469–473.
Dehoux, F., Lecocq, Y., Benhamadouche, S., Manceau, R., Brizzi, L.-E., 2012. Algebraic modelling of the turbulent heat fluxes using the elliptic blending approach - application to forced and mixed convection regimes. Turbulence Combust. 88 (1–2), 77–100.
Dehoux, F., Benhamadouche, S., Manceau, R., 2012. An elliptic blending differential flux model for natural, mixed and forced convection. Int. J. Heat Fluid Flow 63, 190–204.
Duponcheel, M., Bartosiewicz, Y., 2019. Direct numerical simulations of low-prandtl turbulent heat transfer in planar impinging jets. In: The 18th International Topical Meeting on Nuclear Reactor Thermalhydraulics NURETH-18.
Duponcheel, M., Bartosiewicz, Y., 2021. Direct numerical simulation of turbulent heat transfer at low prandtl numbers in planar impinging jets. Int. J. Heat Mass Transf. 173, 121179 https://doi.org/10.1016/j.ijheatmasstransfer.2021.121179.
Duponcheel, M., Bricteux, L., Manconi, M., Winckelmans, G., Bartosiewicz, Y., 2014. Assessment of RANS and improved near-wall modeling for forced convection at low prandtl numbers based on LES up to $Re_\tau = 2000$. Int. J. Heat Mass Transf. 75 (2), 470–482.
Fiore, M., Koloszar, L., Mendez, M.A., Duponcheel, M., Bartosiewicz, Y., 2021a. Thermal turbulence modelling of liquid metal flows via data analysis and machine learning. In: Proceedings of the 12th Symposium of VKI PhD Research, Rhode Saint Genese BE.
Fiore, M., Koloszar, L., Mendez, M.A., Duponcheel, M., Bartosiewicz, Y., 2021. A physics-oriented data-driven approach to thermal turbulence modelling. In: 15th International Conference on Heat Transfer, Fluid Mechanics and Thermodynamics, Virtual Conference, 28–28 July, 2021.
Grötzbach, G., 2011. Revisiting the resolution requirements for turbulence simulations in nuclear heat transfer. Nucl. Eng. Des. 241 (11), 4379–4390.
Grötzbach, G., 2013. Challenges in low-Prandtl number heat transfer simulation and modelling. Nucl. Eng. Des. 264, 41–55.
Hoyas, S., Jimenez, J., 2006. Scaling of the velocity fluctuations in turbulent channels up to $Re_\tau = 2000$. Phys. Fluids 18 (1), 4.
Jiang, C., Mi, J., Laima, S., Li, H., 2020. A novel algebraic stress model with machine-learning-assisted parametrization. Energies 13 (1), 258.
Kader, B.A., 1981. Temperature and concentration profiles in fully turbulent boundary layers. Int. J. Heat Mass Tran. 24.
Kawamura, H., Abe, H., Matsuo, Y., 1999. DNS of turbulent heat transfer in channel flow with respect to Reynolds and Prandtl number effects. Int. J. Heat Fluid Flow 20 (3), 196–207.
Kays, W., 1994. Turbulent Prandtl number – where are we. J. Heat Transfer-Trans. Asme 116 (2), 284–295.
Kenjeres, S., Gunarjo, S.B., Hanjalic, K., 2005. Contribution to elliptic relaxation modelling of turbulent natural and mixed convection. Int. J. Heat Fluid Flow 26 (4), 569–586.
Kolmogorov, A.N., 1941. The local structure of turbulence in incompressible viscous fluid for very large reynolds number. Dokl. Akad. Nauk. SSR 30, 299–303.
Launder, B.E., Sharma, B.I., 1974. Application of the energy-dissipation model of turbulence to the calculation of flow near a spinning disc. Lett. Heat Mass Transfer 1 (2), 131–137.
Leonard, A. Energy cascade in large-eddy simulation of turbulent fluid flows, Ad. Geophys 18A.
Lien, F., Chen, W., Leschziner, M., 1996. Low-reynolds-number eddy-viscosity modelling based on non-linear stress-strain/vorticity relations. In: W. RODI, G. BERGELES (Eds.), Engineering Turbulence Modelling and Experiments, vol. 3 of Elsevier Series in Thermal and Fluid Sciences, Elsevier, Oxford. pp. 91 – 100.
Manceau, R., Hanjalic, K., 2002. Elliptic blending model: a new near-wall reynolds-stress turbulence closure. Phys. Fluids 14 (2), 744–754.
Manservisi, S., Menghini, F., 2014a. A CFD four parameter heat transfer turbulence model for engineering applications in heavy liquid metals. Int. J. Heat Mass Tran. 69, 312–326.
Manservisi, S., Menghini, F., 2014b. Triangular rod bundle simulations of a CFD k-ϵ-k_θ-ϵ_θ) heat transfer turbulence model for heavy liquid metals. Nucl. Eng. Des. 273, 251–270.
A.V. Ortiz, Turbulent natural convection along a vertical plate for different prandtl number fluids, Phd thesis, Université catholique de Louvain, Louvain-la-Neuve, Belgium (2019).
Otic, I., Grötzbach, G., Worner, M., 2005. Analysis and modelling of the temperature variance equation in turbulent natural convection for low-prandtl-number fluids. J. Fluid Mech. 3525, 237–261.
Reynolds, O., 1874. On the extent and action of the heating surface of steam boiler, in. In: Proceedings of the Literary and Philosophical Society of Manchester.
Roelofs, F., 2018. Liquid metal thermal hydraulics: state-of-the art and future perspectives. Nucl. Eng. Des. 362, 110590.
Roelofs, F. (Ed.), 2019. Thermal Hydraulics Aspects of Liquid Metal Cooled Nuclear Reactors. Elsevier, Woodhead Publishing.
Roelofs, F., Shams, A., Otic, I., Böttcher, M., Duponcheel, M., Bartosiewicz, Y., Lakehal, D., Baglietto, E., Lardeau, S., Cheng, X., 2015. Status and perspective of turbulence heat transfer modelling for the industrial application of liquid metal flows. Nucl. Eng. Des. 290, 99–106.
Sagaut, P., 2006. Large eddy simulation for incompressible flows. Springer Science and Business Media.
Santis, A.D., Ortiz, A.V., Shams, A., Koloszar, L., 2019. Modelling of a planar impinging jet at unity, moderate and low prandtl number: assessment of advanced rans closures. Ann. Nucl. Energy 129, 125–145.
Shams, A., Santis, A.D., 2019. Towards the accurate prediction of the turbulent flow and heat transfer in low-prandtl fluids. Int. J. Heat Mass Transf. 130, 290–303.
Shams, A., Roelofs, F., Baglietto, E., Lardeau, S., Kenjeres, S., 2014a. Assessment and calibration of an algebraic turbulent heat flux model for low-Prandtl fluids. Int. J. Heat Mass Transf. 79, 589–601.
Shams, A., Roelofs, F., Baglietto, E., Lardeau, S., Kenjeres, S., 2014b. Assessment and calibration of an algebraic turbulent heat flux model for low-prandtl fluids. Int. J. Heat Mass Tran. 79, 589–601.
Shams, A., Roelofs, F., Niceno, B., Guo, W., Angeli, D., Stalio, E., Fregni, A., Duponcheel, M., Bartosiewicz, Y., Tiselj, I., Oder, J. Reference numerical database for turbulent flow and heat transfer in liquid metals. Nucl. Eng. Des. 353.
Shams, A., De Santis, A., Roelofs, F., 2019b. An overview of the ahfm-nrg formulations for the accurate prediction of turbulent flow and heat transfer in low-prandtl number flows. Nucl. Eng. Des. 355, 110342 https://doi.org/10.1016/j.nucengdes.2019.110342.

Shams, A., De Santis, A., Koloszar, L., Villa Ortiz, A., Narayanan, C., 2019c. Status and perspectives of turbulent heat transfer modelling in low-prandtl number fluids. Nucl. Eng. Design 353, 110220 . https://doi.org/10.1016/j.nucengdes.2019.110220.

Shams, A., Roelofs, F., Tiselj, I., Oder, J., Bartosiewicz, Y., Duponcheel, M., Niceno, B., Guo, W., Stalio, E., Angeli, D., Fregni, A., Buckingham, S., Koloszar, L.K., Ortiz, A.V., Planquart, P., Narayanan, C., Lakehal, D., van Tichelen, K., Jäger, W., Schaub, T., 2019. A collaborative effort towards the accurate prediction of turbulent flow and heat transfer in low-prandtl number fluids. In: The 18th International Topical Meeting on Nuclear Reactor Thermalhydraulics, NURETH-18.

Sotgiu, C., Weigand, B., Semmler, K., Wellinger, P. Towards a general data-driven explicit algebraic reynolds stress prediction framework. Int. J. Heat Fluid Flow 79 (108454).

Stieglitz, R., Schulenberg, T., 2010. Flow measurement techniques in heavy liquid metals. Nucl. Eng. Des. 240, 2077–2087.

Tiselj, I., 2011. DNS of turbulent channel flow at Re_τ=395, 590 and Pr=0.01. In: The 14th International Topical Meeting on Nuclear Reactor Thermalhydraulics NURETH-14.

Tiselj, I., Cizelj, L., 2012. Dns of turbulent channel flow with conjugate heat transfer at prandtl number 0.01. Nucl. Eng. Design 253, 153–160. sI: CFD4NRS-3. doi: 10.1016/j.nucengdes.2012.08.008.

Vasilyev, O., 2000. High order finite difference schemes on non-uniform meshes with good conservation properties. J. Comp. Phys. 157 (2), 746–761.

Yeo, W., 1987. A generalized high pass/low pass filtering procedure for deriving and solving turbulent flow equations (Ph.D. thesis). Ohio State University.